Available online at www.sciencedirect.com
ScienceDirect
Comput. Methods Appl. Mech. Engrg. 391 (2022) 114574
Computer methods in applied mechanics and engineering
www.elsevier.com/locate/cma

On the solution of hyperbolic equations using the peridynamic differential operator

Ali Can Bekar[a], Erdogan Madenci[a,*], Ehsan Haghighat[b,c]

[a] Department of Aerospace and Mechanical Engineering, The University of Arizona, Tucson, AZ 85721, USA
[b] Department of Civil and Environmental Engineering, Massachusetts Institute of Technology, Cambridge, MA 02139, USA
[c] Department of Civil Engineering,University of British Columbia, Vancouver, BC V6T 1Z4, Canada

Received 19 August 2021; received in revised form 28 December 2021; accepted 2 January 2022
Available online 28 January 2022

Abstract

Numerical solution of hyperbolic differential equations, such as the advection equation, poses challenges. Classically, this issue has been addressed by using a scheme known as the upwind scheme. It simply invokes more points from the upwind side of the flow stream when calculating derivatives. This study presents a generalized upwind scheme, referred to as *directional nonlocality*, for the numerical solution of linear and nonlinear hyperbolic Partial Differential Equations (PDEs) using the peridynamic differential operator (PDDO). The PDDO provides the nonlocal form of the differential equations by introducing an internal length parameter (horizon) and a weight function. The weight function controls the degree of interaction among the points within the horizon. A modification to the weight function, i.e., upwinded-weight function, accounts for directional nonlocality along which information travels. This modification results in a stable PDDO discretization of hyperbolic PDEs. Solutions are constructed in a consistent manner without special treatments through simple discretization. The capability of this approach is demonstrated by considering time dependent linear and nonlinear hyperbolic equations as well as the time invariant Eikonal equation. Numerical stability is ensured for the linear advection equation and the PD solutions compare well with the analytical/reference solutions.

Keywords: Peridynamics; Nonlocal; Hyperbolic; Advection; Eikonal

1. Introduction

Hyperbolic partial differential equations (PDEs) are commonly encountered in the modeling of phenomena such as advection, wave transportation, hypersonic flows, mixing flows, atmospheric flows, and hydraulic jumps, etc. Although there exist numerical methods for solving such PDEs, known as the upwind-scheme [1–5], they face challenges if solutions contain discontinuities such as a shock or a contact discontinuity. The challenges arise because the solution does not smooth out with time and discontinuities persist even if the initial and boundary conditions are smooth. However, the discontinuities should be captured and preserved during the solution. Also, the

* Corresponding author.
E-mail addresses: acbekar@email.arizona.edu (A.C. Bekar), madenci@email.arizona.edu (E. Madenci), ehsanh@mit.edu (E. Haghighat).

https://doi.org/10.1016/j.cma.2022.114574
0045-7825/

solution method should ideally preserve the conservation of energy. Therefore, the solution procedure is problem dependent and becomes more of an art.

Although computationally fast and easy to implement, the finite difference methods inherently prone to numerical diffusion and dispersion break down and produce oscillations near the discontinuities such as a shock. Numerical diffusion develops across the contact discontinuity with each time step; it smears out the contact discontinuity during the solution. It is globally nonconservative and requires structured discretization [6]. The finite volume method approximates the spatial derivatives by integrating across a discrete (finite) control volume associated with each grid point while satisfying the integral conservation law for each control volume. It enables the use of unstructured grid; thus, it is suitable for domains with complex geometry. However, it is not easy to implement and is not suitable for Lagrangian models. It also suffers from the presence of discontinuities and higher order of derivatives [7]. The extended finite element method [8] offers an accurate solution for capturing discontinuities, however, tracing discontinuities pose significant challenges within this framework.

A general solution scheme that can handle complex discontinuities for hyperbolic problems is still an open question in computational sciences. The characteristic speed and the direction of the information travel are important when solving hyperbolic PDEs numerically. Therefore, accurate determination of the derivatives of the field variable in the presence of discontinuities and incorporation of the characteristic directions become vital for obtaining the correct solution.

In order to remove these challenges, nonlocal convection equation and nonlocal hyperbolic conservation laws were introduced by employing the peridynamic nonlocal operators. Tian et al. [9] proposed a non-local convection–diffusion model using finite element approximation and compared upwind and symmetric kernel cases. They observed that the symmetric kernel model generates unnecessary oscillations; however, the upwind model is more stable. Leng et al. [10] presented a Petrov–Galerkin method for the nonlocal convection dominated diffusion problem using a spherical and a hemispherical interaction region. Lee and Du [11] extended the nonlocal modeling by stating that symmetry of the non-local interaction is not essential for nonlocal modeling. Also, Lee and Du [12] created two Smooth Particle Hydrodynamic (SPH) models using upwind kernel and a nonlocal viscous term by borrowing them from local theory and concluded that their method is inherently stable. Du et al. [13] introduced a nonlocal model for conservation laws with monotonicity preserving and entropy stable properties. Also, Du et al. [14] considered nonlinear conservation laws using nonlocal theory. Du et al. [15] considered initial volume-constrained problems encountered for linear nonlocal convection–diffusion equation.

The Peridynamic differential operator (PDDO) introduced by Madenci et al. [16–18] also provides the nonlocal form of hyperbolic PDEs by introducing an internal length parameter (horizon) and a weight function. It enables numerical differentiation through integration; thus, the field equations are valid everywhere regardless of the presence of discontinuities. It simply considers the interaction between the neighboring points for the evaluation of derivatives. The weight function controls the degree of association among the points within the horizon. This study introduces an upwinded-weight function based on the knowledge of characteristic directions along which information travels. This form of the weight function enables the solution of hyperbolic PDEs using the PDDO; the solution procedure is no longer problem dependent.

Solutions to challenging linear and nonlinear multi-dimensional hyperbolic PDEs are constructed in a consistent manner without special treatments. It captures the discontinuities with simple discretization. Furthermore, it enables the imposition of periodic boundary conditions without any additional constraint conditions. The capability of this approach is demonstrated by considering time dependent linear and nonlinear hyperbolic equations as well as the time independent nonlinear Eikonal equation. Numerical stability is ensured analytically for the linear advection equation and numerically for all other problems, and solutions compare well with the analytical/reference solutions.

2. Hyperbolic equations

The hyperbolic partial differential equations arise in many problems including wave transportation, hypersonic flows and advection problem, resulting in different form of PDEs. This study concerns two classes of first-order hyperbolic equations: time dependent PDEs arising in problems such as advection and time-invariant PDEs arising in problems such as the Eikonal equation.

2.1. First order time-dependent

The general form of time dependent and first-order hyperbolic system of equations of conservative type can be stated as

$$\frac{\partial \mathbf{Q}}{\partial t} + \frac{\partial \mathbf{F}}{\partial \mathbf{x}} = 0 \tag{1a}$$

or

$$\frac{\partial \mathbf{Q}}{\partial t} + \mathbf{J}\frac{\partial \mathbf{Q}}{\partial \mathbf{x}} = 0 \tag{1b}$$

subjected to the initial condition

$$\mathbf{Q}(\mathbf{x}, t = 0) = \mathbf{f}(\mathbf{x}) \tag{2}$$

and Dirichlet and Neumann boundary conditions

$$\mathbf{Q}(\mathbf{x}, t) = \mathbf{g}_D(\mathbf{x}, t) \tag{3a}$$

and

$$\nabla \mathbf{Q}(\mathbf{x}, t) \bullet \mathbf{n} = \mathbf{g}_N(\mathbf{x}, t) \tag{3b}$$

where $\mathbf{Q}$ is a vector of unknown field variables, $\mathbf{F} = \mathbf{F}(\mathbf{Q})$ is the flux vector and $\mathbf{J} = \frac{\partial \mathbf{F}}{\partial \mathbf{Q}}$ is the Jacobian matrix with real and distinct eigenvalues. The known functions, $\mathbf{f}(\mathbf{x})$, $\mathbf{g}_D(\mathbf{x}, t)$ and $\mathbf{g}_N(\mathbf{x}, t)$ represent the specified initial and boundary conditions, respectively. The eigenvalues correspond to the characteristic speeds of the system and the eigenvectors provide the directions of information travel. The characteristic speeds (eigenvalues) should be recovered when solving these equations numerically.

2.2. First order time-invariant

In geophysics, a time independent first order nonlinear hyperbolic PDE known as the Eikonal equation describes the traveltime, $T = T(\mathbf{x})$ of propagating compression waves under the acoustic assumption. It is subjected to a constraint at the source location as $T(\mathbf{x}_s) = 0$. For an isotropic medium, it is of the form [19]

$$\left(\frac{\partial T}{\partial x}\right)^2 + \left(\frac{\partial T}{\partial y}\right)^2 + \left(\frac{\partial T}{\partial z}\right)^2 = \frac{1}{\upsilon^2(\mathbf{x})} \tag{4}$$

in which $\upsilon(\mathbf{x})$ is the known velocity field. It is subjected to a constraint at the source location as $T(\mathbf{x}_s) = 0$. The information travels with a direction depending on the source location or the direction of wave propagation.

3. Peridynamic differential operator

Madenci et al. [16–18] introduced the Peridynamic Differential Operator (PDDO) to construct the nonlocal representation of a scalar field $f = f(\mathbf{x})$ and its derivatives at point $\mathbf{x}$ by considering its interactions with the other points, $\mathbf{x}'$, in its interaction domain known as horizon, as shown in red in Fig. 1. It provides differentiation of Nth order in M dimensions through integration without a medium smoothness requirement.

The derivation of PDDO utilizes concept of PD interactions [20] and construction of PD functions that are orthogonal to each term in the Taylor Series Expansion (TSE). In the discretized domain, each point has its own family members. The points $\mathbf{x}$ and $\mathbf{x}'$ only interact with the other points in their own interaction domains, $H_{\mathbf{x}}$ and $H_{\mathbf{x}'}$, respectively. The relative position vector between these points is defined as $\boldsymbol{\xi} = \mathbf{x}' - \mathbf{x}$. The interaction domains for points $\mathbf{x}$ and $\mathbf{x}'$ do not need to be symmetric, which makes PDDO an attractive method for variety of problems.

Since only the first order spatial derivatives of the field variable appear in Eqs. (1) and (4), its TSE is expressed as

$$f(\mathbf{x} + \boldsymbol{\xi}) = f(\mathbf{x}) + \xi_x \frac{\partial f(\mathbf{x})}{\partial x} + \xi_y \frac{\partial f(\mathbf{x})}{\partial y} + \xi_z \frac{\partial f(\mathbf{x})}{\partial z} + R_1(\mathbf{x}) \tag{5}$$

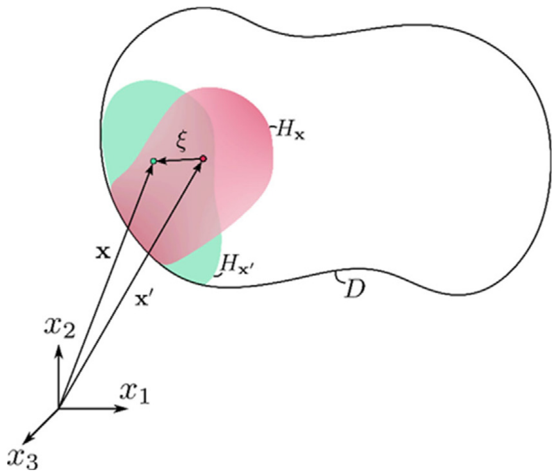

Fig. 1. The PD interaction domains, a.k.a. horizons, red and green, with arbitrary shape and size, for the discretized points $\mathbf{x}$ and $\mathbf{x}'$, respectively. (For interpretation of the references to color in this figure legend, the reader is referred to the web version of this article.)

where $\mathbf{x}^T = \{x, y, z\}$, ξ_x, ξ_y and ξ_z are the components of the vector, $\boldsymbol{\xi}$ and $R_1(\mathbf{x})$ represents the remainder of the 1st order approximation. Multiplying each term with PD functions, $g_1^{r_x r_y r_z}(\boldsymbol{\xi})$ and integrating over the domain of interaction (family), $H_{\mathbf{x}}$ result in

$$\int_{H_{\mathbf{x}}} f(\mathbf{x}+\boldsymbol{\xi}) g_1^{r_x r_y r_z}(\boldsymbol{\xi}) dV_{\mathbf{x}'} = f(\mathbf{x}) \int_{H_{\mathbf{x}}} g_1^{r_x r_y r_z}(\boldsymbol{\xi}) dV_{\mathbf{x}'} + \frac{\partial f(\mathbf{x})}{\partial x} \int_{H_{\mathbf{x}}} \xi_x g_1^{r_x r_y r_z}(\boldsymbol{\xi}) dV_{\mathbf{x}'} + \frac{\partial f(\mathbf{x})}{\partial y} \int_{H_{\mathbf{x}}} \xi_y g_1^{r_x r_y r_z}(\boldsymbol{\xi}) dV_{\mathbf{x}'} + \frac{\partial f(\mathbf{x})}{\partial z} \int_{H_{\mathbf{x}}} \xi_z g_1^{r_x r_y r_z}(\boldsymbol{\xi}) dV_{\mathbf{x}'} \quad (6)$$

The PD functions must be orthogonal to each term in the TSE as

$$\int_{H_{\mathbf{x}}} \xi_x^{s_x} \xi_y^{s_y} \xi_z^{s_z} g_1^{r_x r_y r_z}(\boldsymbol{\xi}) dV_{\mathbf{x}'} = \delta_{s_x r_x} \delta_{s_y r_y} \delta_{s_z r_z} \quad (7)$$

in which $\delta_{s_i r_i}$ with $(i = x, y, z)$ is the Kronecker delta symbol and the super and subscripts are defined as $s_x, s_y, s_z, r_x, r_y, r_z = 0, 1$. Applying the orthogonality conditions, Eq. (7) results in PD form of the function itself and its first order derivatives as

$$f^{PD}(\mathbf{x}) = \int_{H_{\mathbf{x}}} f(\mathbf{x}+\boldsymbol{\xi}) g_1^{000}(\boldsymbol{\xi}) dV_{\mathbf{x}'} \quad (8)$$

and

$$\begin{Bmatrix} f_{,x}^{PD} \\ f_{,y}^{PD} \\ f_{,z}^{PD} \end{Bmatrix} = \int_{H_{\mathbf{x}}} f(\mathbf{x}+\boldsymbol{\xi}) \begin{Bmatrix} g_1^{100}(\boldsymbol{\xi}) \\ g_1^{010}(\boldsymbol{\xi}) \\ g_1^{001}(\boldsymbol{\xi}) \end{Bmatrix} dV_{\mathbf{x}'}. \quad (9)$$

As detailed in Madenci et al. [18], the 1st order PD functions can be constructed using linear polynomial basis functions as

$$g_1^{r_x r_y r_z}(\boldsymbol{\xi}) = a_{000}^{r_x r_y r_z} w(|\boldsymbol{\xi}|) + a_{x00}^{r_x r_y r_z} w(|\boldsymbol{\xi}|)\xi_x + a_{0y0}^{r_x r_y r_z} w(|\boldsymbol{\xi}|)\xi_y + a_{00z}^{r_x r_y r_z} w(|\boldsymbol{\xi}|)\xi_z \quad (10)$$

where $a_{q_x q_y q_z}^{r_x r_y r_z}$ with $(q_x, q_y, q_z = 0, x, y, z)$ are the unknown coefficients and $w(|\boldsymbol{\xi}|)$ is the non-dimensional weight function which controls the strength of interactions among the family members. It may vary from point to point and as discussed subsequently, and can also be modified to invoke directional nonlocality based on the direction of information travel. Substituting the PD functions back into the orthogonality equation, Eq. (7) after algebraic manipulations leads to a system of equations which determines the coefficients as

$$\mathbf{A}\mathbf{a} = \mathbf{b} \quad (11)$$

in which

$$\mathbf{A}=\int_{H_{\mathbf{x}}} w(|\boldsymbol{\xi}|)\begin{bmatrix}1 & \xi_x & \xi_y & \xi_z \\ \xi_x & \xi_x^2 & \xi_x\xi_y & \xi_x\xi_z \\ \xi_y & \xi_y\xi_x & \xi_y^2 & \xi_y\xi_z \\ \xi_z & \xi_z\xi_x & \xi_z\xi_y & \xi_z^2\end{bmatrix} dV_{\mathbf{x}'} \tag{12}$$

$$\mathbf{a}=\begin{bmatrix} a_{000}^{000} & a_{000}^{100} & a_{000}^{010} & a_{000}^{001} \\ a_{x00}^{000} & a_{x00}^{100} & a_{x00}^{010} & a_{x00}^{001} \\ a_{0y0}^{000} & a_{0y0}^{100} & a_{0y0}^{010} & a_{0y0}^{001} \\ a_{00z}^{000} & a_{00z}^{100} & a_{00z}^{010} & a_{00z}^{001}\end{bmatrix} \tag{13}$$

and

$$\mathbf{b}=\begin{bmatrix}1 & 0 & 0 & 0 \\ 0 & 1 & 0 & 0 \\ 0 & 0 & 1 & 0 \\ 0 & 0 & 0 & 1\end{bmatrix}. \tag{14}$$

Determination of the unknown coefficients through $\mathbf{a}=\mathbf{A}^{-1}\mathbf{b}$ establishes the PD functions $g_1^{r_x r_z}(\boldsymbol{\xi})$. The derivations and pertinent computer programs are given by Madenci et al. [18].

The weight function dictates the degree of nonlocality among the material points within the family of each point. Any nondimensional weight function is mathematically acceptable; however, in reality, the influence of the weight function should reflect the decrease in the degree of interaction with increasing distances, and the characteristics of the differential equation describing a physical phenomena. In the previous studies [16–18], the weight function has been specified as a Gaussian distribution in the form of

$$w\left(|\boldsymbol{\xi}|;\delta\right)=e^{-4(|\boldsymbol{\xi}|/\delta)^2} \tag{15}$$

in which the horizon, δ defines the extent of domain of interaction, $H_{\mathbf{x}}$ for point $\mathbf{x}$. However, this particular form results in an unstable solution scheme for the solution of hyperbolic equations. To resolve this issue and motivated by the classical upwind scheme, the weight function is modified as $w\left(|\boldsymbol{\xi}|,\kappa^{\pm};\delta\right)$ expressed as

$$w\left(|\boldsymbol{\xi}|,\kappa^{\pm};\delta\right)=\kappa^{\pm}e^{-4(|\boldsymbol{\xi}|/\delta)^2} \tag{16}$$

where the parameter $\kappa^{\pm}$ allows for the information travel from $+$ and $-$ directions as illustrated in Figs. 2 and 3 for linear and nonlinear conservation laws, respectively. This particular form provides a simple way to reflect the effect of upwinding direction and to control the degree of interaction between the points. This modification is sufficient to arrive at a stable PDDO discretization of hyperbolic equations. In order to satisfy the entropy condition for nonlinear hyperbolic conservation laws, the influence of downwind family members is completely disregarded as shown in Fig. 3. However, this is not necessary for linear conservation law as shown in Fig. 2. Therefore, small influence from downwind material points is included in order to ensure invertibility of matrix, $\mathbf{A}$ in Eq. (12).

In practice, increasing the influence of upwind material points and decreasing the influence of the downwind material points is sufficient for numerical stability for the linear problems and the values of κ can be flexible in value. For specified values of κ, the stability limit of the method is presented in Section 5.1. For nonlinear problems, downwind coefficients are specified as zero in order to satisfy the entropy condition which ensures that method is conservative, consistent and monotonicity preserving as shown Section 5.2.

4. Numerical implementation

The integrals are evaluated through a meshless quadrature technique. Considering a uniform grid spacing of Δ, the size of the horizon can be defined as $\delta=m\Delta$, with m as the number of family points in each direction. To have a stable discretization, m should be selected such that $N\leq m\leq N+2$, with $N=1$ as the highest order spatial

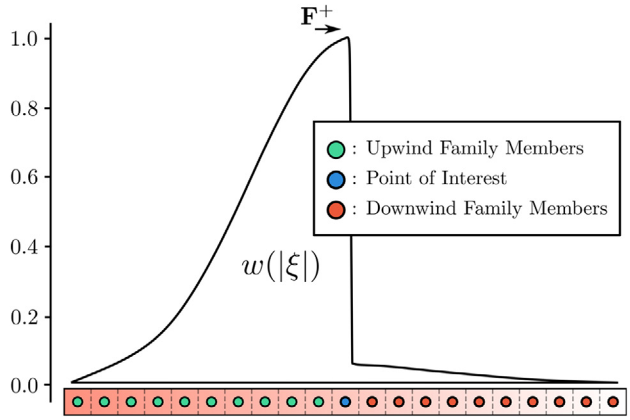

Fig. 2. Degree of interaction among the points for $\boldsymbol{F}^+$ for linear conservation laws.

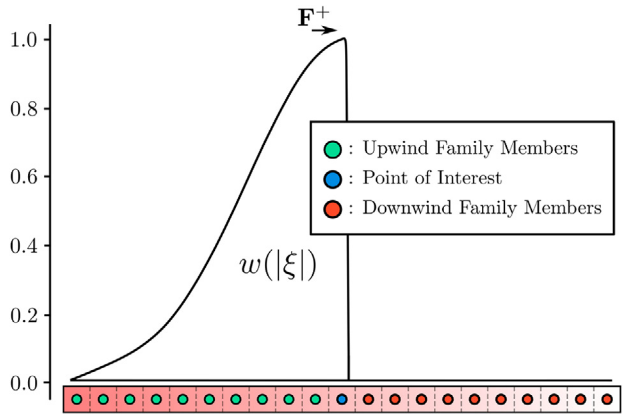

Fig. 3. Degree of interaction among the points for $\boldsymbol{F}^+$ for nonlinear conservation laws.

derivative appearing in the PDE. For a fixed value of m, the PD representation must converge to the local form as the parameter δ approaches zero. As shown in Fig. 4., the interior points can have a symmetric family. However, the boundary points always have a nonsymmetric family.

The discretized form of Eqs. (8) and (9) are expressed as

$$f^{PD}(\mathbf{x}_{(k)}) = \sum_{j=1}^{N_{(k)}} f(\mathbf{x}_{(j)}) g_1^{000}(\mathbf{x}_{(j)} - \mathbf{x}_{(k)}) V_{(j)} \quad \text{for} \quad k = 1, \ldots, K \tag{17}$$

and

$$\begin{Bmatrix} f_{,x}^{PD}(\mathbf{x}_{(k)}) \\ f_{,y}^{PD}(\mathbf{x}_{(k)}) \\ f_{,z}^{PD}(\mathbf{x}_{(k)}) \end{Bmatrix} = \sum_{j=1}^{N_{(k)}} f(\mathbf{x}_{(j)}) \begin{Bmatrix} g_1^{100}(\mathbf{x}_{(j)} - \mathbf{x}_{(k)}) \\ g_1^{010}(\mathbf{x}_{(j)} - \mathbf{x}_{(k)}) \\ g_1^{001}(\mathbf{x}_{(j)} - \mathbf{x}_{(k)}) \end{Bmatrix} V_{(j)} \text{ for } k = 1, \ldots, K \tag{18}$$

in which $V_{(j)}$ represents the volume of each point, $\mathbf{x}_{(j)}$ and $N_{(k)}$ denote the number of family members of point $\mathbf{x}_{(k)}$. Thus, the summation accounts for all of the interactions of point $\mathbf{x}_{(k)}$ within its family. The Gaussian quadrature rule is employed with unit integration weights. The total number of grid points in the computational domain is denoted by K. In order to invoke the direction of information travel during the solution, the PD functions are constructed by employing the upwinded weight function. The family member construction is achieved by the KD-tree algorithm [21].

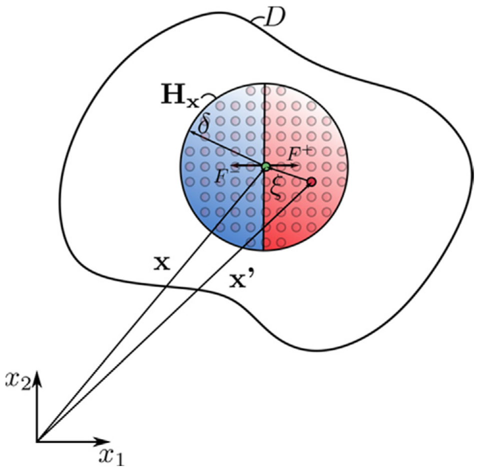

Fig. 4. Domain of interaction for point **x** with directional nonlocality.

The boundary conditions are imposed through a boundary layer with a depth Δ along the boundary of the region. As introduced by Madenci et al. [22], the periodic boundary conditions are enforced by simply completing the family of a point near the boundary as shown in Fig. 6.

The convergence of the nonlocal PD differentiation to exact local differentiation can be achieved as the horizon decreases and the number of integration points increases with decreasing grid space, Δx. This type convergence is known as $\delta-$ convergence as suggested by Bobaru et al. [23]. In order to minimize the error, the appropriate value for each variable is determined based on the $\delta-$ convergence. The convergence study is performed by considering different horizon size, δ, grid spacing, Δx and number of family members, m. For a fixed value of m, the PD solution must converge to the local solution as the parameter δ approaches zero.

The convergence criteria is based on two measures. For time dependent hyperbolic PDEs, an error metric with L_1 norm is defined as

$$\varepsilon = \frac{\left| u_m^{(e)} - u_m^{(c)} \right|_1}{\left| u_m^{(e)} \right|_1} \tag{19}$$

For the Eikonal equation, the global error measure is defined as

$$\varepsilon = \frac{1}{\left| u^{(e)} \right|_{\max}} \sqrt{\frac{1}{K} \sum_{m=1}^{K} \left[u_m^{(e)} - u_m^{(c)} \right]^2} \tag{20}$$

in which the superscripts e and c denote the exact and the numerical solutions, respectively. The parameter, K represents the total number of collocation points in the domain. The convergence rate for the solution of each problem type is established based on the error measure.

One of the major advantages of this approach is that it can be applied to any type of hyperbolic equation without any special treatment. The method is rather advantageous in the presence of severe variations in the field. Also, it enables the construction of the nonlocal form of any type of flux function. Its implementation is not complicated for those familiar with other numerical methods such as the Finite Element Method or the Finite Difference Method, with the algorithms provided by Madenci et al. [18]. Furthermore, it is suitable for parallelization since the discrete form of the equations results in a system of algebraic equations. The GPU architecture can accelerate the computations significantly [24]. In a recent study, the PDDO has been applied to the solution of rather challenging nonlinear PDEs such as Burgers, Swift–Hohenberg, Korteweg–de Vries, Kuramoto–Sivashinsky, nonlinear Schrödinger, and Cahn–Hilliard equations [25]. Therefore, this method can be applied to higher order and multidimensional hyperbolic systems because PDDO has the ability to approximate higher order derivatives with great accuracy.

5. Numerical results

The numerical results demonstrate the capability and robustness of the PDDO for solving linear and nonlinear hyperbolic PDEs by considering the following equations: (1) Linear advection equation, (2) Inviscid Burgers equation, (3) Euler equations of gas dynamics, and (4) Eikonal equation for traveltime.

5.1. Linear advection equation

Linear advection equation modeling the transportation of an incompressible fluid by a known velocity can be expressed as

$$\frac{\partial u}{\partial t} + \upsilon \frac{\partial u}{\partial x} = 0 \text{ for } 0 \leq x \leq L = 4 \text{ with } t > 0 \tag{21}$$

in which υ is the known advection velocity and u is the unknown motion of a scalar field. It is subjected to a periodic boundary condition as

$$u\,(x = 0, t) = u\,(x = L, t) \tag{22}$$

The initial condition is specified as

$$u\,(x, t = 0) = H(x - 1.5) - H(x - 2.5) \tag{23}$$

where $H(x - x_0)$ is the Heaviside step function. The analytical solution to this equation is of the form [26]

$$u\,(x, t) = u(x - \upsilon t, t) \tag{24}$$

By employing Euler's first order explicit time integration (EE) and PDDO for spatial derivative, Eq. (21) is converted to a system of algebraic equations in terms of the PD unknowns, $u_{(k)}^{t+\Delta t} = u^{t+\Delta t}(x_{(k)})$ as

$$u_{(k)}^{t+\Delta t} = u_{(k)}^{t} - \upsilon \Delta t \left(\sum_{j=1}^{N_{(k)}} u_{(j)}^{t}\, {}^{+}g_1^1(\xi_{(k)(j)})\ell_{(j)} \right) \text{ for } k = 1, \ldots, K = 401. \tag{25}$$

The solution is constructed by considering a uniform grid spacing of $\Delta = 0.01$ with a horizon size of $\delta = 2\Delta$ and a time step size of $\Delta t = 0.01$. As illustrated in Fig. 6, the periodic boundary condition is enforced by completing the family of a point near the boundary.

The direction of information travel depends on the sign (characteristic direction) of the known velocity, υ as shown in Fig. 7. The vector, $\boldsymbol{\upsilon}$ indicates the characteristic direction. Therefore, the PD functions, ${}^{+}g_1^1(\xi_{1(k)(j)})$ are constructed by using the upwinded weight function with directional nonlocality (upwinding) as

$$w\left(|\xi|, \kappa^{+}; \delta\right) = \kappa^{+} e^{-4(|\xi|/\delta)^2} \tag{26}$$

where

$$\kappa^{+} = \begin{cases} 0.0 & \text{if} \quad \xi < 0 \\ 1.0 & \text{if} \quad \xi \geq 0 \end{cases} \tag{27}$$

Fig. 8 shows the comparison of the PD solution with the analytical solution for $0 \leq t \leq 4$. It is clear that the numerical dissipation exists; however, it is stable and not excessive as shown in Fig. 9. Also, the PD solution captures the characteristic speed. Furthermore, the form of the initial condition as a step function is preserved in future time steps.

Numerical stability analysis is performed by considering the scalar field at time $(t + \Delta t)$ as

$$u^{t+\Delta t}(x_{(k)}) = e^{\alpha(t+\Delta t)} e^{imx_{(k)}} \tag{28}$$

where $i = \sqrt{-1}$, α is a real variable and m is a positive integer. Its substitution into Eq. (25) after certain algebraic manipulations results in

$$e^{\alpha \Delta t} = 1 - \frac{\upsilon \Delta t}{\Delta x} \left(\sum_{j=1}^{N_{(k)}} e^{im(\xi_{kj})} C_k \right) = \mathrm{Re}(G) + i\,\mathrm{Im}(G) \tag{29}$$

For unconditional stability, von Neumann condition requires that the amplification factor, $\left|e^{\alpha\Delta t}\right|$ satisfy the following condition

$$\left|e^{\alpha\Delta t}\right| = \sqrt{(\mathrm{Re}(G))^2 + (\mathrm{Im}(G))^2} \leq 1 \tag{30}$$

Fig. 10 shows that stability limit and convergence for varying horizon sizes. It is stable for a weight function with directional nonlocality. The stability limit is established by the maximum value of the Courant number $C = \upsilon\Delta t/\Delta x$ which makes $\left|e^{\alpha\Delta t}\right| < 1$. Its maximum is determined as $\max(\upsilon\Delta t/\Delta x) \approx 1.2$ for $\delta = 2\Delta$x.

For a symmetric weight function, it can be cast into the following form as

$$\left|e^{\alpha(\Delta t)}\right| = 1 + \frac{\upsilon^2\Delta t^2}{\Delta x^2} H(m, \Delta x) \tag{31}$$

where $H(m, \Delta x)$ is defined as

$$H(m, \Delta x) = \sin^2(m\Delta x)\left[0.0382\cos^2(m\Delta x) + 0.9653 + 0.3842\cos(m\Delta x)\right] \tag{32}$$

Its derivative evaluation shows that $H(m, \Delta x) \geq 0$ for any m and Δx. Therefore, it is unconditionally unstable for a weight function without directional nonlocality. Also, Fig. 11 shows that $H(m, \Delta x)$ has nonnegative values for all $m\Delta x \in [0, 2\pi]$.

Convergence properties of the solution is examined by considering a smooth initial condition such as $\sin(\pi x)$ with the same Courant number of $C = 1$. Fig. 12 shows the expected linear convergence rate of about unity for the first order PDEs. The error, ε in Eq. (19) is measured against the analytical solution at $t = 2$.

5.2. Inviscid Burgers equation

The inviscid Burgers equation allows modeling of complex shock and refraction waves. As previously considered by [7], it is stated as

$$\frac{\partial u}{\partial t} + u\frac{\partial u}{\partial x} = 0 \text{ for} 0 \leq x \leq L = 2 \quad \text{for} \quad t > 0 \tag{33}$$

In conservative form, it can be written as

$$\frac{\partial u}{\partial t} + \frac{\partial F}{\partial x} = 0 \tag{34}$$

in which u is the unknown scalar field and $F = u^2/2$. It is subjected to a periodic boundary condition of the form

$$u\,(x = 0, t) = u\,(x = L, t) \tag{35}$$

The initial condition is specified as

$$u\,(x, t = 0) = \sin \pi x \tag{36}$$

Characteristic directions do not change; it can be positive or negative. It has an analytical solution of the from [27] and solution at the desired timestep can be obtained by following characteristic information

$$u\,(x, t) = \sin(\pi x - ut) \tag{37}$$

By employing Euler's first order explicit time integration and PDDO for spatial derivative, Eq. (33) is converted to a system of algebraic equations in terms of the PD unknowns, $u_{(k)}^{t+\Delta t} = u^{t+\Delta t}(x_{(k)})$ as

$$u_{(k)}^{t+\Delta t} = u_{(k)}^{t} - \frac{\Delta t}{2}\left(\sum_{j=1}^{N_{(k)}} \left(u_{(k)(j)}^{t}\right)^2 {}^{\pm}g_1^1(\xi_{1(k)(j)})\ell_{(j)}\right) \quad \text{for} \quad k = 1, \ldots, K = 201. \tag{38}$$

As illustrated in Fig. 5, the periodic boundary condition is enforced by completing the family of a point near the boundary. The solution is constructed by considering a uniform grid spacing of $\Delta = 0.01$ with a horizon size of $\delta = 2\Delta$ and a time step size of $\Delta t = 0.001$.

The direction of information travel depends on the sign of the field variable, ${}^{\pm}u$. Therefore, the PD functions, ${}^{\pm}g_1^1(\xi_{1(k)(j)})$ are constructed by using a weight function with directional nonlocality as

$$w\left(|\boldsymbol{\xi}|, \kappa^{\pm}; \delta\right) = \kappa^{\pm} e^{-4(|\boldsymbol{\xi}|/\delta)^2} \tag{39}$$

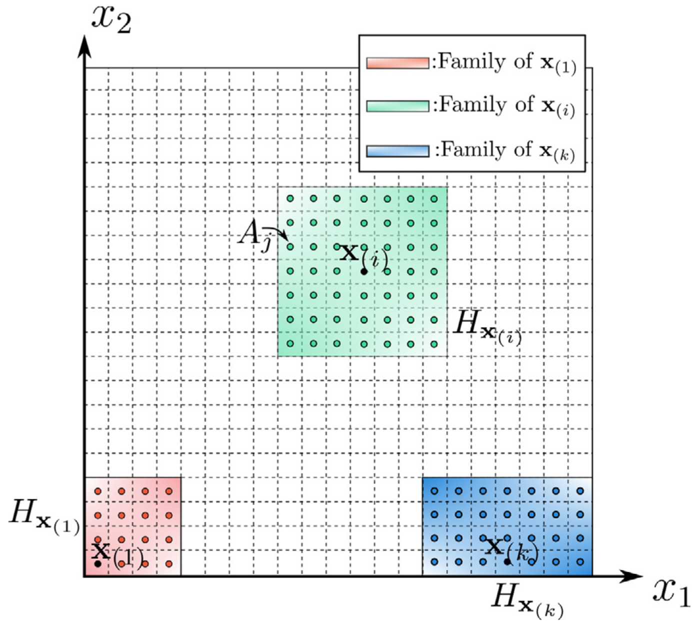

Fig. 5. Description of families in a PD computational domain.

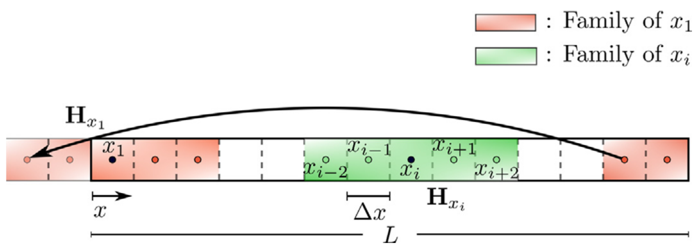

Fig. 6. Transfer of information to complete the families of points near the boundary.

where

$$\kappa^+ = \begin{cases} 0.0 & \text{if} \quad \xi < 0 \\ 1.0 & \text{if} \quad \xi \geq 0 \end{cases} \text{ in the region } u^+ \tag{40}$$

and

$$\kappa^- = \begin{cases} 1.0 & \text{if} \quad \xi < 0 \\ 0.0 & \text{if} \quad \xi \geq 0 \end{cases} \text{ in the region } u^- \tag{41}$$

Regions, u^+ and u^- shown in Fig. 13 indicate the characteristic directions dictated by the sign of the field variable.

The PD solution is stable and captures the shock formation without any special treatment and remains single valued. Fig. 14 shows a close agreement between the PD and numerical WENO technique with 4th the order Runge–Kutta method (RK4) [28]. It is a high-order approach with non-oscillatory behavior. The PD solution based on a straightforward time integration scheme compares well with the results from a high order method employing a multi-step integration technique. The characteristic directions collide and form a shock and remains single valued as shown in Fig. 15.

Shock occurrence time (break) time is $t_b = (1/\pi)$; therefore, the error, ε in Eq. (19) is measured against the characteristic solution prior to this time with a Courant number of $C = 1$. As expected, the convergence rate shown in Fig. 16 is close to unity.

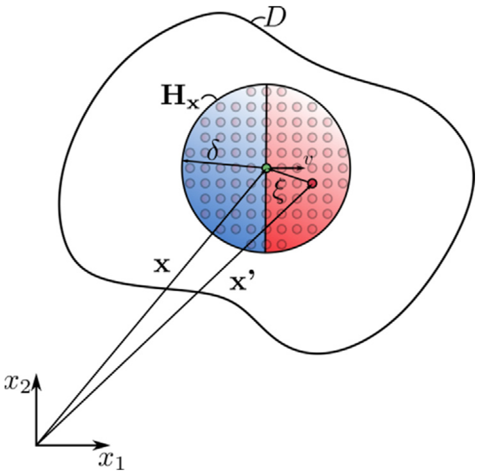

Fig. 7. Direction of information travel (upwinding) in domain of interaction for point **x** for linear advection equation.

The method should satisfy entropy condition in order to ensure the convergence of solution. Hence, it must be conservative, consistent and monotonicity preserving because it is first order. The influence from downwind material points can be completely disregarded for nonlinear conservation laws if κ values in the weight function, Eq. (16) are specified as

$$\kappa^{+} = \begin{cases} 0 & \text{if} \quad \boldsymbol{\xi} \bullet \boldsymbol{v} < 0 \\ 1.0 & \text{if} \quad \boldsymbol{\xi} \bullet \boldsymbol{v} \geq 0 \end{cases} \tag{42}$$

By employing Euler's first order explicit time integration (EE) and PDDO for spatial derivative with a horizon size of $\delta = 2\Delta$, Eq. (33) is converted to a system of algebraic equations in terms of the PD unknowns, $u_{(k)}^{t+\Delta t} = u^{t+\Delta t}(x_{(k)})$ as

$$u_{(k)}^{t+\Delta t} = u_{(k)}^{t} - \frac{\Delta t}{2\Delta x}\left[0.8994\left(u_{(k)}^{t}\right)^2 - 0.7987\left(u_{(k-1)}^{t}\right)^2 - 0.1006\left(u_{(k-2)}^{t}\right)^2\right] \tag{43}$$

It is worth noting that the summation of the coefficients of the flux terms associated with each family member vanishes. The flux over a domain is only a function of inlet and outlet fluxes; therefore, the method is conservative.

The values of $u_{(k)}^{t+\Delta t}$, $u_{(k-1)}^{t}$ and $u_{(k-2)}^{t}$ can be approximated based on TSE as

$$u_{(k)}^{t+\Delta t} \approx u_{(k)}^{t} + \frac{\partial u}{\partial t}\Delta t \tag{44a}$$

$$u_{(k-1)}^{t} \approx u_{(k)}^{t} - \frac{\partial u}{\partial x}\Delta x \tag{44b}$$

and

$$u_{(k-2)}^{t} \approx u_{(k)}^{t} - \frac{\partial u}{\partial x}2\Delta x. \tag{44c}$$

Substituting from Eq. (44) into Eq. (43) results in

$$\frac{u_{(k)}^{t} + \frac{\partial u}{\partial t} - u_{(k)}^{t}}{\Delta t} + \frac{1}{2\Delta x}\left[0.8994\left(u_{(k)}^{t}\right)^2 - 0.7987\left(u_{(k)}^{t} - \frac{\partial u}{\partial x}\Delta x\right)^2 - 0.1006\left(u_{(k)}^{t} - \frac{\partial u}{\partial x}2\Delta x\right)^2\right] = 0 \tag{45}$$

After some modifications, this expression can be recast as

$$\begin{aligned} &\frac{\partial u}{\partial t} + \frac{1}{2\Delta x}\left(2 \times 0.7987 u_{(k)}^{t}\frac{\partial u}{\partial x}\Delta x + 4 \times 0.1006 u_{(k)}^{t}\frac{\partial u}{\partial x}\Delta x\right) \\ &-\frac{1}{2\Delta x}\left(0.7987\left(\frac{\partial u}{\partial x}\Delta x\right)^2 + 0.1006\left(\frac{\partial u}{\partial x}2\Delta x\right)^2\right) = 0 \end{aligned} \tag{46}$$

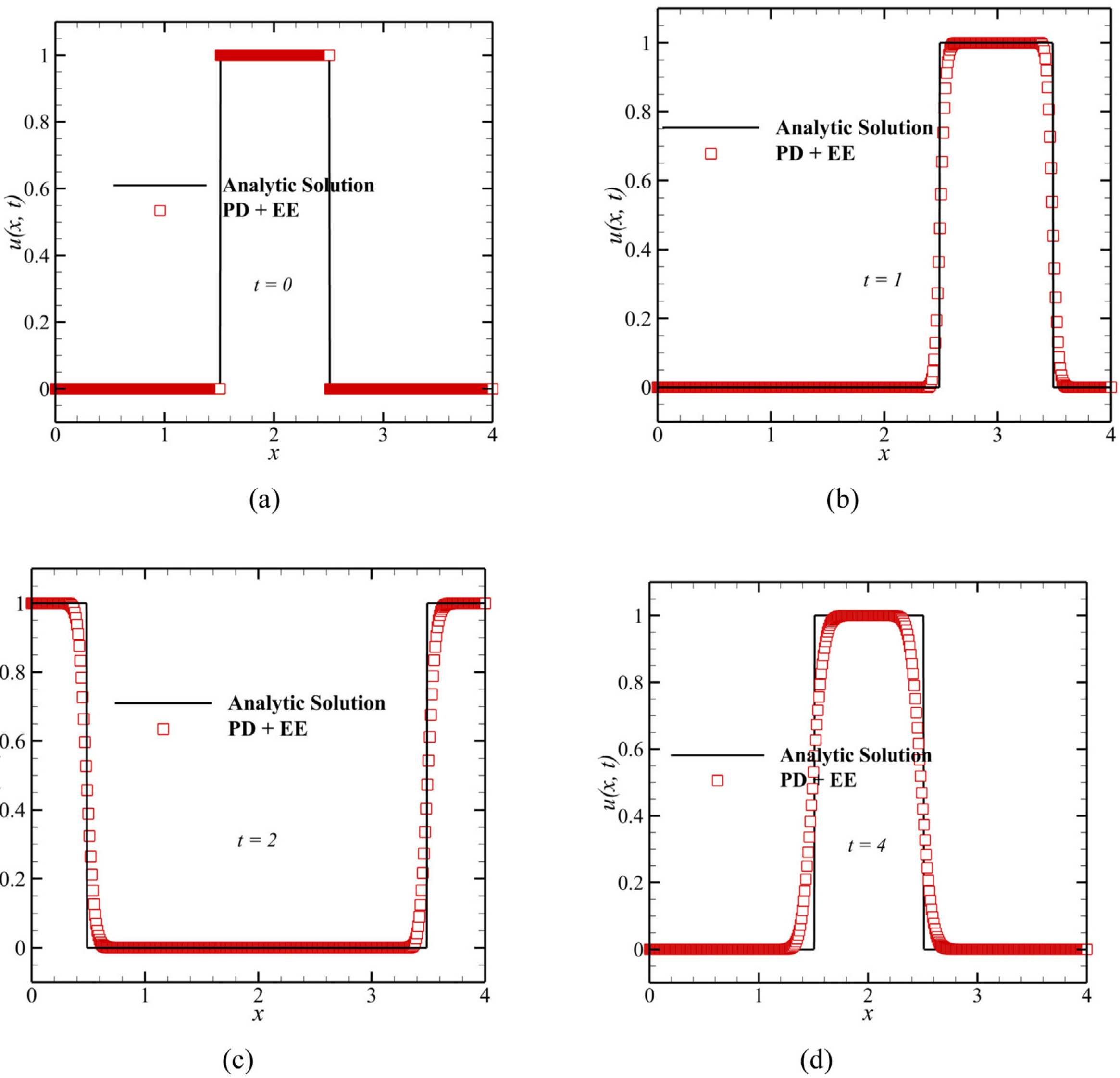

Fig. 8. Comparison of PD and analytical solutions for linear-advection equation as time progresses (a) $t = 0$, (b) $t = 1$, (c) $t = 2$, and (d) $t = 4$.

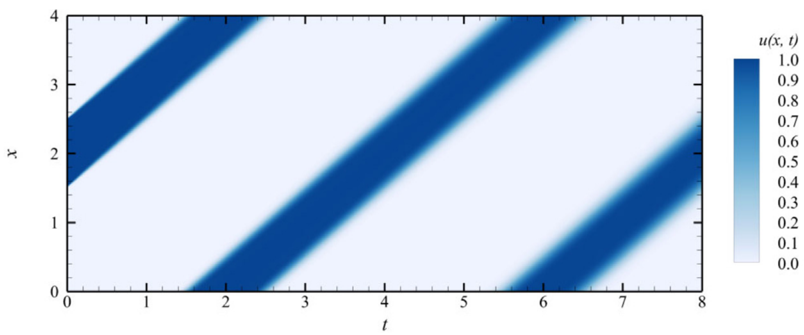

Fig. 9. PD solution of linear advection equation.

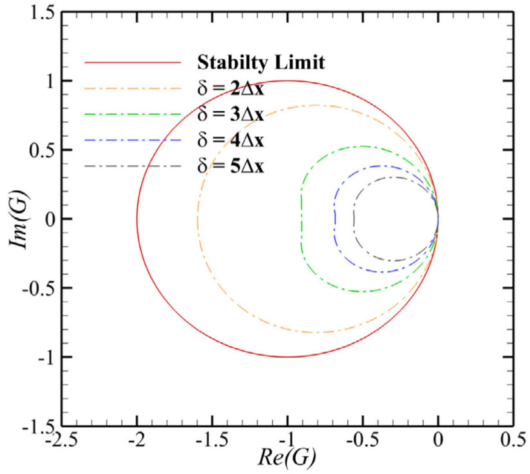

Fig. 10. Numerical stability of linear advection equation solution for varying horizon and directional nonlocality.

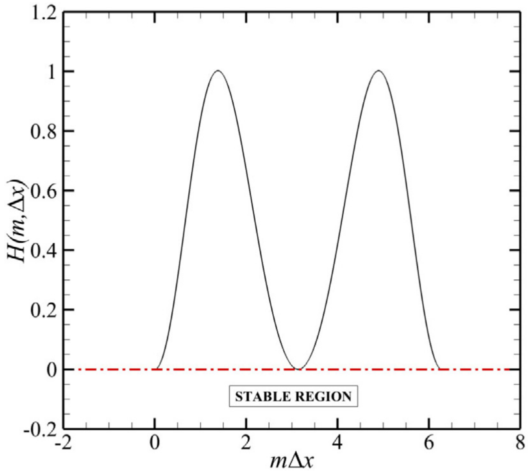

Fig. 11. Nonnegative variation of $H(m, \Delta x)$ without directional nonlocality for $m\Delta x \in [0, 2\pi]$.

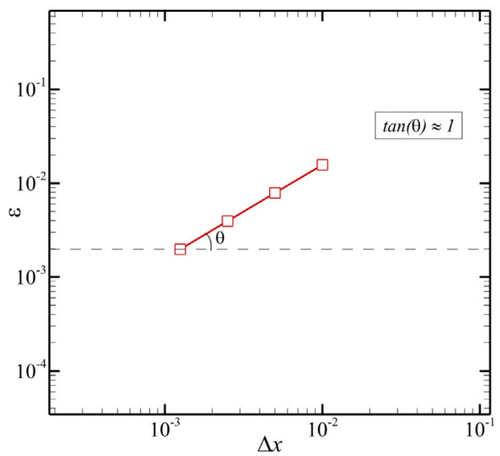

Fig. 12. Convergence behavior of linear advection equation for a varying grid size.

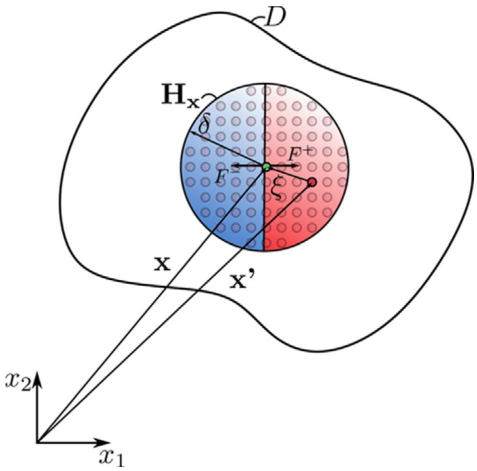

Fig. 13. Domain of interaction for point **x** depending on positive and negative characteristic directions.

in which the last term go to zero as $\Delta x \rightarrow 0$ and canceling out Δx in the second term results in

$$\frac{\partial u}{\partial t}+u\frac{\partial u}{\partial x}\approx 0 \tag{47}$$

The discrete version of the equation converges to the analytic form, Eq. (33) as both Δt and $\Delta x \rightarrow 0$. Therefore, the method is consistent. Higher order terms are disregarded since they include higher powers of Δt or Δx as multipliers. The remainder terms or products of remainder terms also satisfies the consistency condition.

The method is monotonicity preserving if it satisfies the well-known following condition [26]

$$\frac{\partial u_{(k)}^{t+\Delta t}}{\partial u_{(k)}^{t}}\geq 0 \tag{48}$$

If the left hand side is assumed as the upwind direction, i.e., $u_{(k-1)}^{t}>0$ and $u_{(k-2)}^{t}>0$, the following condition is obtained from Eq. (43) for monotonicity preserving

$$\frac{1}{0.8994}>\frac{\Delta t}{\Delta x}u_{(k)}^{t} \tag{49}$$

or a more strict condition can be defined as

$$1.1>\frac{\Delta t}{\Delta x}\left|\max(u)\right| \tag{50}$$

Provided that this condition is satisfied, the PDDO method is conservative, consistent and monotonicity preserving; thus, entropy stable.

5.3. Euler equations of gas dynamics

In conservative form, the equations of gas dynamics can be stated as [6]

$$\frac{\partial \mathbf{Q}}{\partial t}+\frac{\partial \mathbf{F}}{\partial x}=0 \quad \text{for } 0\leq x\leq 10 \tag{51}$$

where the vectors **Q** and **F** are defined as

$$\mathbf{Q}=\begin{bmatrix}\rho\\ \rho u\\ E\end{bmatrix} \text{ and } \mathbf{F}=\begin{bmatrix}\rho u\\ \rho u^2+p\\ (E+p)\,u\end{bmatrix} \tag{52}$$

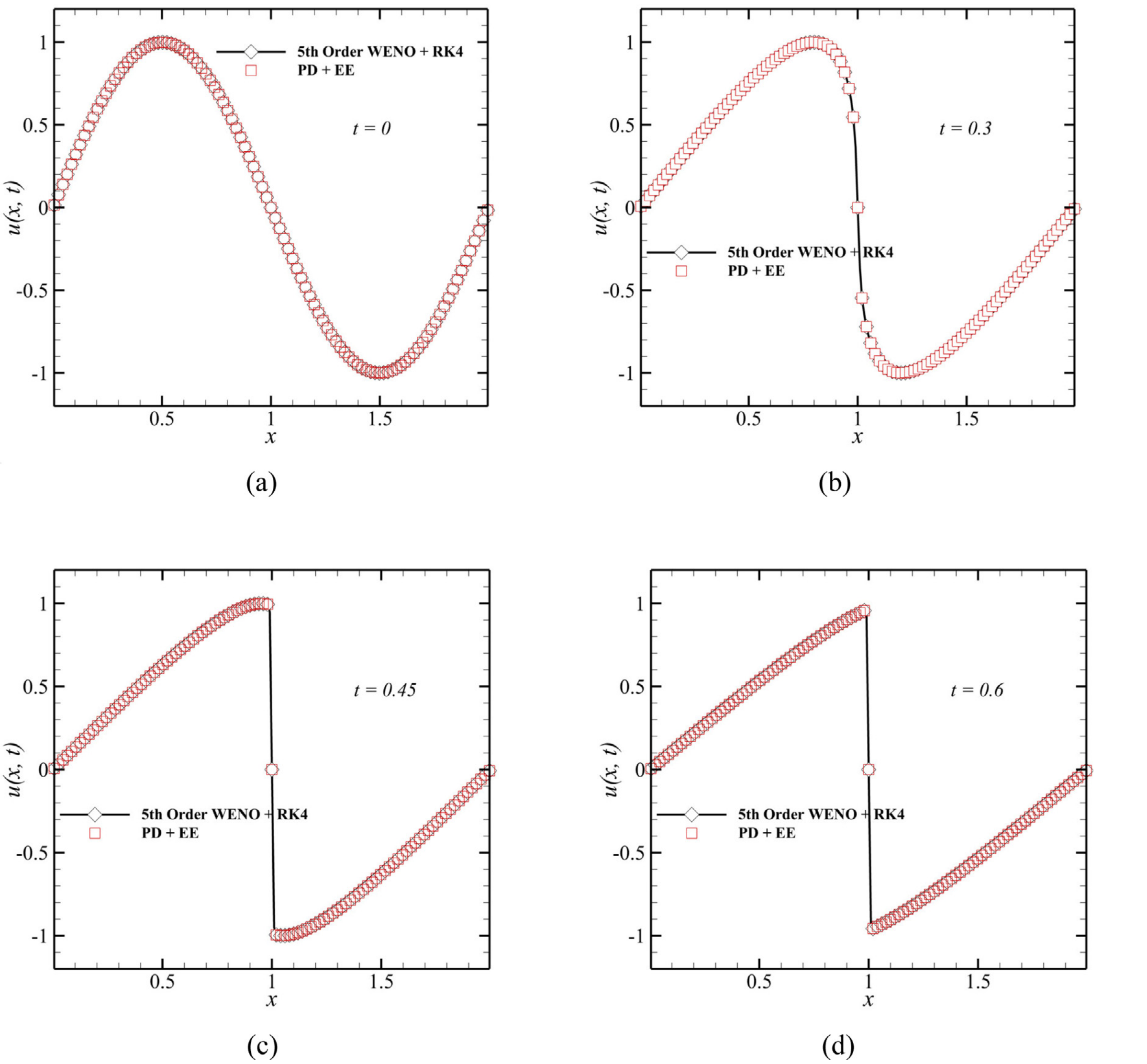

Fig. 14. Comparison of PD and analytical solutions for inviscid Burgers equation as time progresses (a) $t = 0$, (b) $t = 0.3$, (c) $t = 0.45$, and (d) $t = 0.6$.

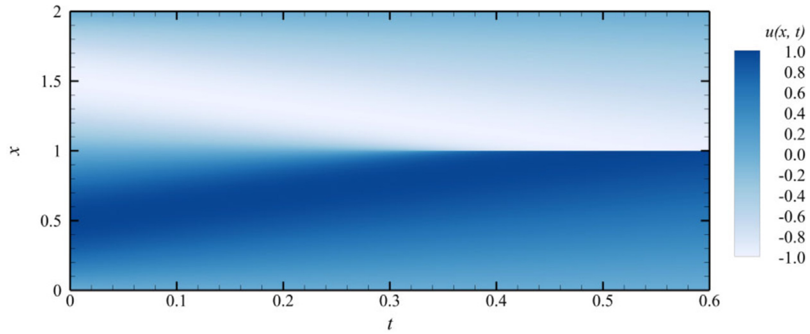

Fig. 15. PD solution of inviscid Burgers equation.

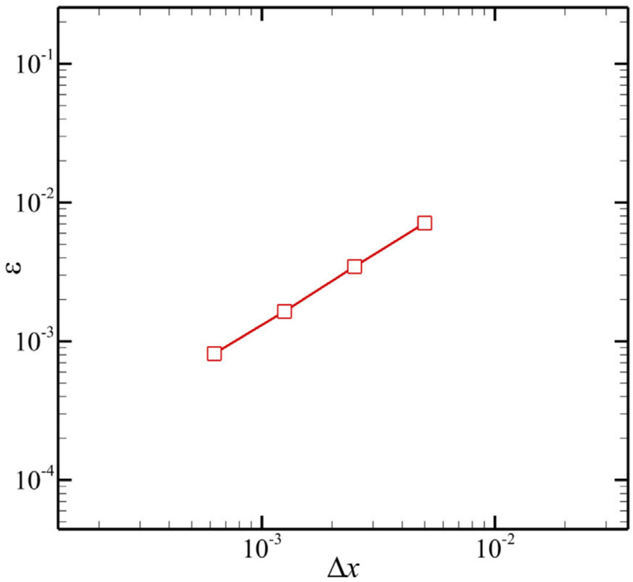

Fig. 16. Convergence behavior of Burgers equation for varying grid size.

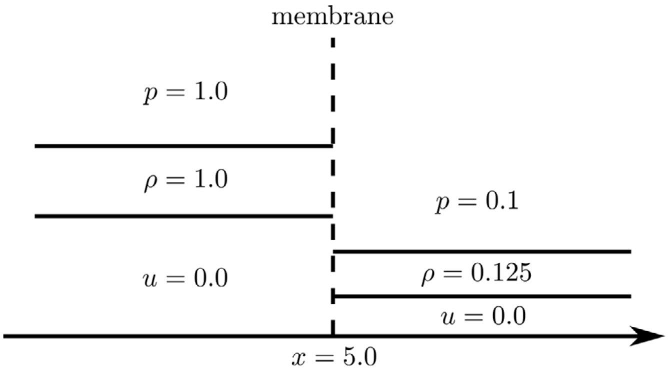

Fig. 17. Initial conditions for Sod's shock tube problem.

where density, velocity and pressure ρ, u and p, respectively, represent the primitive variables. The internal energy per unit mass, e and total energy per unit volume, E are defined as

$$e = \frac{p}{\rho\,(\gamma - 1)} \tag{53}$$

and

$$E = \rho e + \frac{1}{2}\rho u^2 \tag{54}$$

with the gas constant, $\gamma = 1.4$.

The initial condition consists of high density and pressure on the left, low density and pressure on the right and zero velocity on both sides of the membrane in Sod's shock tube as shown in Fig. 17. The analytical solution is available in [6].

It can be recast as

$$\frac{\partial \mathbf{Q}}{\partial t} + \mathbf{J}\frac{\partial \mathbf{Q}}{\partial x} = 0 \quad \text{for } 0 \leq x \leq 10 \tag{55}$$

where the Jacobian matrix $\mathbf{J}$ is determined as

$$\mathbf{J} = \begin{bmatrix} u & \rho & 0 \\ 0 & u & 1/\rho \\ 0 & \gamma\rho & u \end{bmatrix} \tag{56}$$

Its distinct eigenvalues are $\lambda^- = u + c$, $\lambda_0 = u$ and $\lambda^+ = u - c$ with $c = \sqrt{\gamma p/\rho}$ representing the adiabatic speed of sound. One of them only depends on the direction of fluid velocity, and the other two depend on the fluid velocity and speed of sound (acoustic waves). The corresponding eigenvectors representing the characteristic directions are

$$\mathbf{r}^+ = \begin{Bmatrix} -\rho/c \\ 1 \\ -\rho c \end{Bmatrix}, \mathbf{r}_0 = \begin{Bmatrix} 1 \\ 0 \\ 0 \end{Bmatrix} \text{ and } \mathbf{r}^- = \begin{Bmatrix} \rho/c \\ 1 \\ \rho c \end{Bmatrix} \tag{57}$$

Based on the flux splitting method introduced by Van Leer [29], the flux vector is split as

$$\mathbf{F} = \mathbf{F}^+ + \mathbf{F}^- \tag{58}$$

in which

$$\mathbf{F}^+ = \frac{\rho}{4c}(u+c)^2 \begin{bmatrix} 1 \\ \dfrac{(\gamma-1)\,u + 2c}{\gamma} \\ \dfrac{[(\gamma-1)\,u+2c]^2}{2\left(\gamma^2-1\right)} \end{bmatrix} \text{ and } \mathbf{F}^- = -\frac{\rho}{4c}(u-c)^2 \begin{bmatrix} 1 \\ \dfrac{(\gamma-1)\,u - 2c}{\gamma} \\ \dfrac{[2c-(\gamma-1)\,u]^2}{2\left(\gamma^2-1\right)} \end{bmatrix} \tag{59}$$

With this splitting, Eq. (51) can be recast as

$$\frac{\partial \mathbf{Q}}{\partial t} + \frac{\partial(\mathbf{F}^+ + \mathbf{F}^-)}{\partial x} = 0 \text{ for } 0 \le x \le 10 \tag{60}$$

By employing Euler's first order explicit time integration and PDDO for spatial derivative, Eq. (60) is converted to a system of algebraic equations in terms of the PD unknowns, $\mathbf{Q}_{(k)}^{t+\Delta t} = \mathbf{Q}^{t+\Delta t}(x_{(k)})$ as

$$\mathbf{Q}_k^{t+\Delta t} = \mathbf{Q}_k^t - \sum_{j=1}^{N_{(k)}} \mathbf{F}_{(k)(j)}^{+}\,{}^{+}g_1^1(\xi_{1(k)(j)})A_{(j)} - \sum_{j=1}^{N_{(k)}} \mathbf{F}_{(k)(j)}^{-}\,{}^{-}g_1^1(\xi_{1(k)(j)})\ell_{(j)} \text{ for } k = 1, \ldots, K = 101. \tag{61}$$

The solution is constructed by considering a uniform grid spacing of $\Delta = 0.01$ with a horizon size of $\delta = 2\Delta$ and a time step size of $\Delta t = 0.01$.

Consistent with the splitting (direction of information travel), the PD functions, ${}^{\pm}g_1^1(\xi_{1(k)(j)})$ for $\mathbf{F}^+$ and $\mathbf{F}^-$ are constructed by using the weight function with directional nonlocality shown in Fig. 18 as

$$w\left(|\xi|, \kappa^{\pm}; \delta\right) = \kappa^{\pm} e^{-4(|\xi|/\delta)^2} \tag{62}$$

in which

$$\kappa^+ = \begin{cases} 0.0 & \text{if} \quad \xi < 0 \\ 1.0 & \text{if} \quad \xi \ge 0 \end{cases} \text{ in the region } \mathbf{F}^+ \tag{63}$$

and

$$\kappa^- = \begin{cases} 1.0 & \text{if} \quad \xi < 0 \\ 0.0 & \text{if} \quad \xi \ge 0 \end{cases} \text{ in the region } \mathbf{F}^- \tag{64}$$

Regions, $\mathbf{F}^+$ and $\mathbf{F}^-$ shown in Fig. 18 indicate the characteristic directions dictated by the sign of the field variable.

The PD predictions capture the analytical solution [6] as shown in Fig. 19. It captures the shock and rarefaction without any special treatment. As evident in the solution for density, it is composed of a shock propagating to the right, while a left-going rarefaction forms. In between these two waves, there is a jump in the density, which is the contact discontinuity. It accurately captures the shock and contact discontinuities.

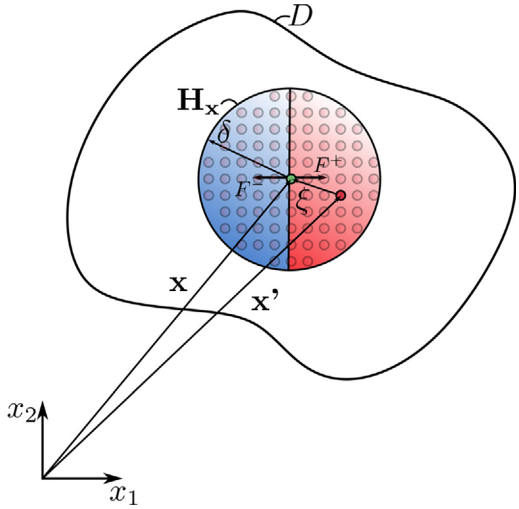

Fig. 18. Domain of interaction for point $\mathbf{x}$ depending on the flux splitting directions.

5.4. Eikonal equation

The isotropic Eikonal equation for travel time, $T = T(x, y, z)$ is of the form [19]

$$\left(\frac{\partial T}{\partial x}\right)^2 + \left(\frac{\partial T}{\partial y}\right)^2 + \left(\frac{\partial T}{\partial z}\right)^2 = \frac{1}{\upsilon^2(x, y, z)} \text{ for } (x, y, z) \in [0, L = 0.5 \text{ km}] \tag{65}$$

in which $\upsilon(x, y, z)$ is the known velocity field. It is subjected to a constraint at the source location, $\mathbf{x}_s = (0.25, 0.25, 0.25)$ as $T(\mathbf{x}_s) = 0$. The velocity field shown in Fig. 20, has constant velocity gradient in $z-$ direction as $g_z = 1.0 \text{ s}^{-1}$ and $\upsilon(\mathbf{x}_s) = 2.25$ km/s. The analytical solution is of the form [19]

$$T(\mathbf{x}) = \frac{1}{\sqrt{g_z^2}} \cosh^{-1}\left(1 + \frac{g_z^2 |\mathbf{x} - \mathbf{x}_s|^2}{2\upsilon(\mathbf{x})\, \upsilon(\mathbf{x}_s)}\right) \tag{66}$$

Replacing the local derivatives with their PD counterparts in the Eikonal equation leads to its discrete form as

$$\begin{aligned} &\left(\sum_{j=1}^{N_{(k)}} T_{(k)(j)} g_1^{100}(\xi_{1(k)(j)}, \xi_{2(k)(j)}, \xi_{3(k)(j)}) V_{(j)}\right)^2 + \left(\sum_{j=1}^{N_{(k)}} T_{(k)(j)} g_1^{010}(\xi_{1(k)(j)}, \xi_{2(k)(j)}, \xi_{3(k)(j)}) V_{(j)}\right)^2 + \\ &\left(\sum_{j=1}^{N_{(k)}} T_{(k)(j)} g_1^{001}(\xi_{1(k)(j)}, \xi_{2(k)(j)}, \xi_{3(k)(j)}) V_{(j)}\right)^2 = \frac{1}{\upsilon^2(x, y, z)} \text{ for } k = 1, \ldots, K \end{aligned} \tag{67}$$

where K is the total number of PD points in the discretization. Similarly, the condition $T(\mathbf{x}_s) = 0$ can be discretized as

$$T(x_s, y_s, z_s) = \sum_{j=1}^{N_{(s)}} T_{(s)(j)} g_1^{000}(\xi_{1(s)(j)}, \xi_{2(s)(j)}, \xi_{3(s)(j)}) V_{(j)} = 0 \tag{68}$$

This constraint condition is enforced by deleting the corresponding row in the resulting system of equations.

The weight function is updated depending on the location of the point inside the family and the gradient direction of the travel time at the point of interest as illustrated in Fig. 21. It is expressed as

$$w(|\xi|, \kappa; \delta) = \kappa e^{-4(|\xi|/\delta)^2} \tag{69}$$

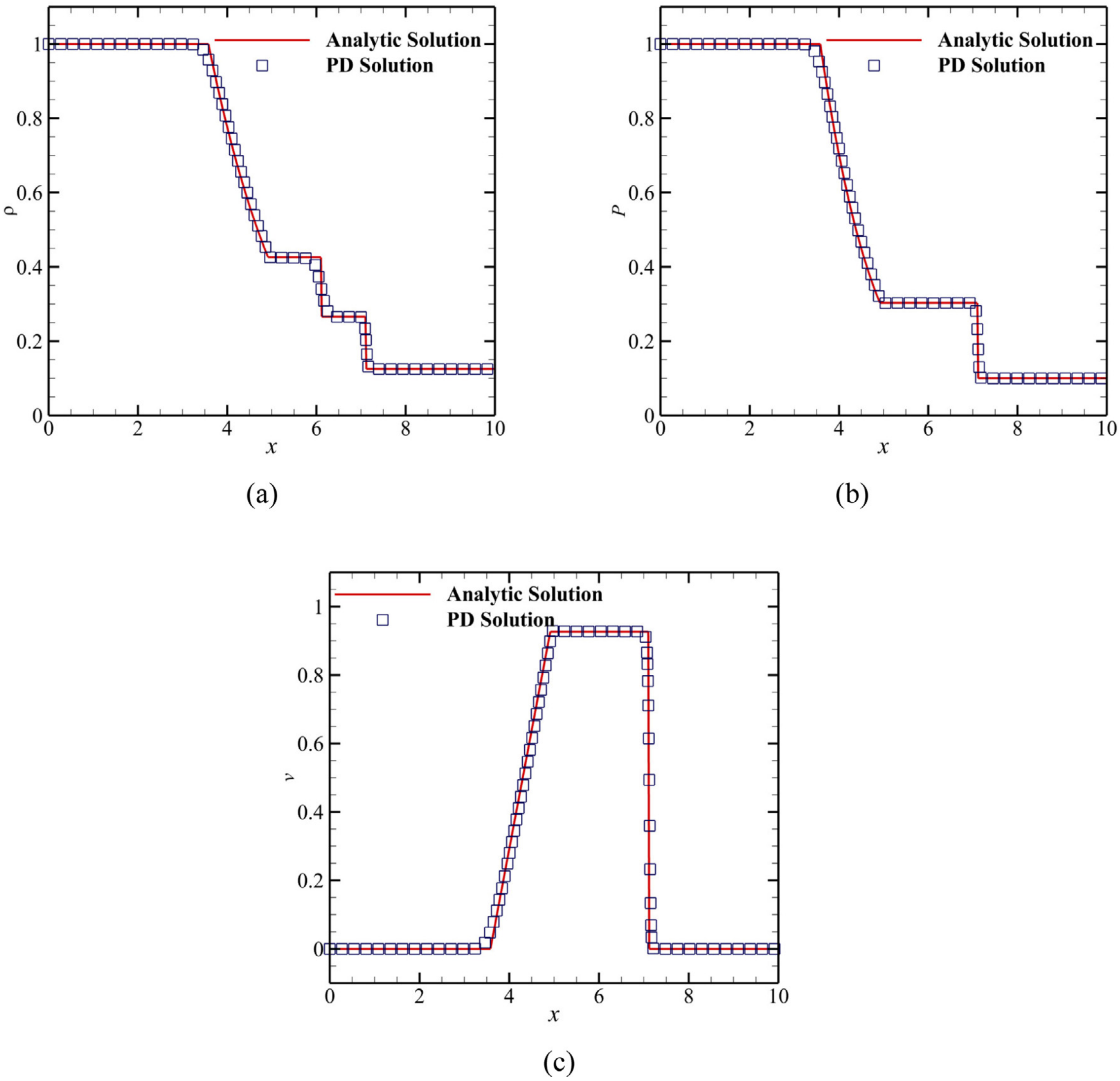

Fig. 19. PD solutions for the Sod shock tube: (a) density, (b) pressure, and (c) velocity at $t = 1.2$.

with

$$\kappa = \begin{cases} 0.1 & \text{if} \quad \boldsymbol{\xi} \cdot \nabla T < 0 \\ 1.0 & \text{if} \quad \boldsymbol{\xi} \cdot \nabla T \geq 0 \end{cases} \tag{70}$$

The domain is discretized with uniform grid spacing of $\Delta = 0.01$ km in each direction with $k = 1, \ldots, K = 51 \times 51 \times 51$. The solution to this non-linear system of algebraic equations is constructed by considering a horizon size of $\delta = 2\Delta$.

The resulting non-linear algebraic system of equations can be expressed as

$$\mathbf{F}(\mathbf{u}) = \mathbf{0} \tag{71}$$

in which the vector $\mathbf{u}$ contains the PD unknowns, $T(\mathbf{x}_{(j)})$ at each point. The nonlinear equations can be solved by employing the Newton–Raphson method in an iterative manner. Hence, the solution can be expressed through a

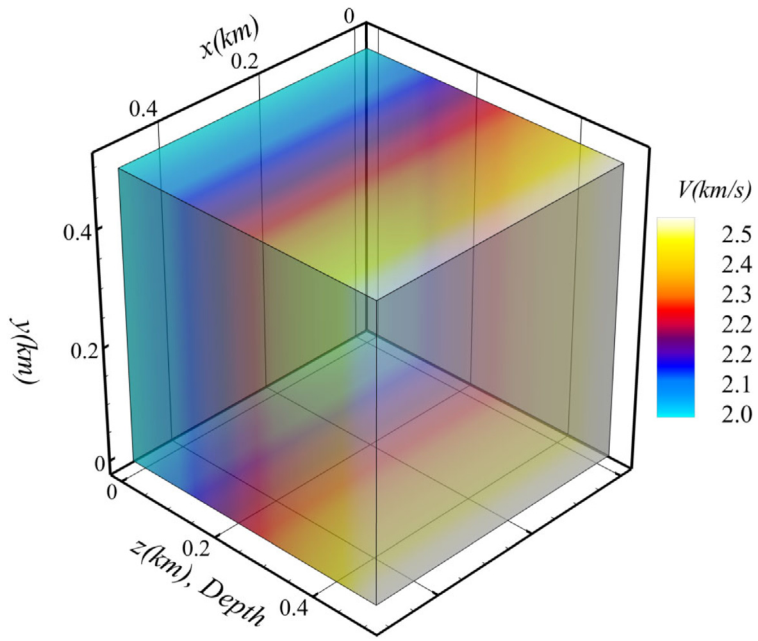

Fig. 20. Velocity field with a uniform gradient in the z-direction.

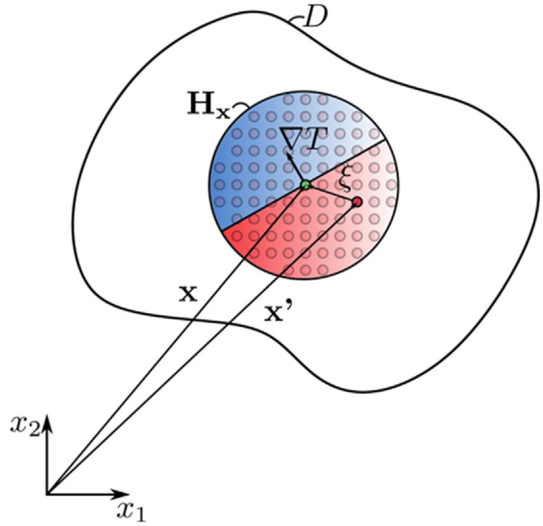

Fig. 21. Weight function with directional nonlocality for the Eikonal equation.

recursive form as

$$\left(\frac{\partial \mathbf{F}}{\partial \mathbf{u}}\right)^{(n)} \Delta \mathbf{u}^{(n+1)} = -\mathbf{F}(\mathbf{u}^{n}) \tag{72}$$

or

$$\Delta \mathbf{u}^{(n+1)} = -\mathbf{J}^{-1}(\mathbf{u}^{(n)})\mathbf{F}(\mathbf{u}^{n}) \tag{73}$$

with

$$\mathbf{J}(\mathbf{u}^{(n)}) = \frac{\partial \mathbf{F}(\mathbf{u}^{(n)})}{\partial \mathbf{u}} \tag{74}$$

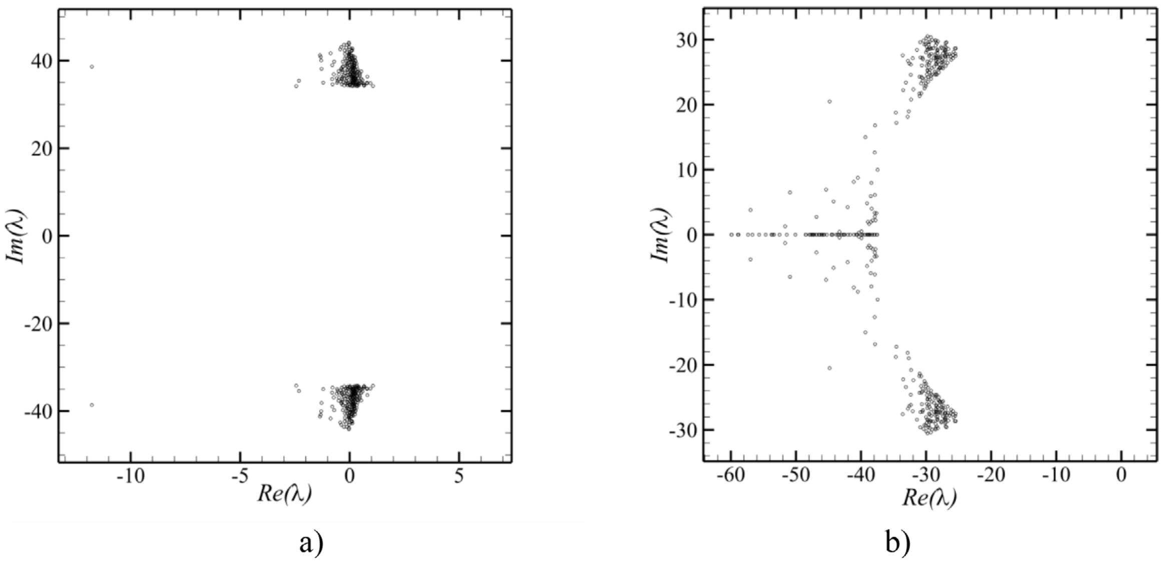

Fig. 22. Real and imaginary parts of the eigenvalues of $-\mathbf{J}$ corresponding weight function: (a) without directional nonlocality (symmetric), and (b) with directional nonlocality.

in which $\mathbf{u}^{(n+1)} = \mathbf{u}^{(n)} + \Delta\mathbf{u}^{(n+1)}$ with n representing the iteration number in the algorithm and $\Delta\mathbf{u}^{(n+1)}$ the incremental unknown vector.

The boundedness of the solution $\mathbf{u}$ depends on the behavior of $-\mathbf{J}^{-1}$. Therefore, the method is stable if the real parts of all eigenvalues of $-\mathbf{J}^{-1}$ are negative. Otherwise, it is unstable. It is worth noting that the real parts of the eigenvalues of $-\mathbf{J}^{-1}$ and $-\mathbf{J}$ have the same signs. Therefore, examining the eigen spectrum of $-\mathbf{J}$ is sufficient. Fig. 22 shows the real and imaginary parts of the eigenvalues of $-\mathbf{J}$ corresponding to the weight function with and without directional nonlocality. The Jacobian, $-\mathbf{J}$ corresponds to the %2 randomly perturbed analytical solution of the isotropic Eikonal equation. The weight function with directional nonlocality results in eigenvalues with only negative real parts. However, the symmetric weight function without directional nonlocality results in eigenvalues with both positive and negative real parts. This ascertains the stability and necessity of the modification of the symmetric weight function using the gradient of the travel times. Also, the weight function with directional nonlocality ensures the numerical stability of the solution procedure [30].

Initial guess is specified as spheres with different radii centered at the source location in the form

$$T_{init} = \frac{(x-0.25)^2 + (y-0.25)^2 + (z-0.25)^2}{2} \tag{75}$$

The Jacobian matrix is evaluated through automatic differentiation, and the equations are solved by employing the Generalized Minimal RESidual method (GMRES) with ILU preconditioner. Depending on the position of family members and the gradient direction of the traveltime, the weight function and the PD functions are updated during each iteration. The convergence of solution is achieved when $\|\mathbf{F}(\mathbf{u})\| < 1.5 \times 10^{-3}$. As shown in Fig. 23, the PD solution captures the analytical solution. The error measure, Eq. (20) of PD solution against the reference solution is relatively uniform as shown in Fig. 24.

6. Conclusions

The study presents the first attempt in the application of the PDDO to solve challenging hyperbolic PDEs. PDDO converts the local form of differential equations to their nonlocal form with an internal parameter that defines the extent of nonlocal effects. Here, a modified weight function, referred to upwinded-weight function, is introduced that invokes the direction of information travel (upwinding) in a natural way. This choice results in a stable PDDO discretization for the solution of such problems. The PDDO can be paired with well-known flux splitting methods in a consistent manner. Numerical stability is always ensured and the solutions to these equations are achieved in

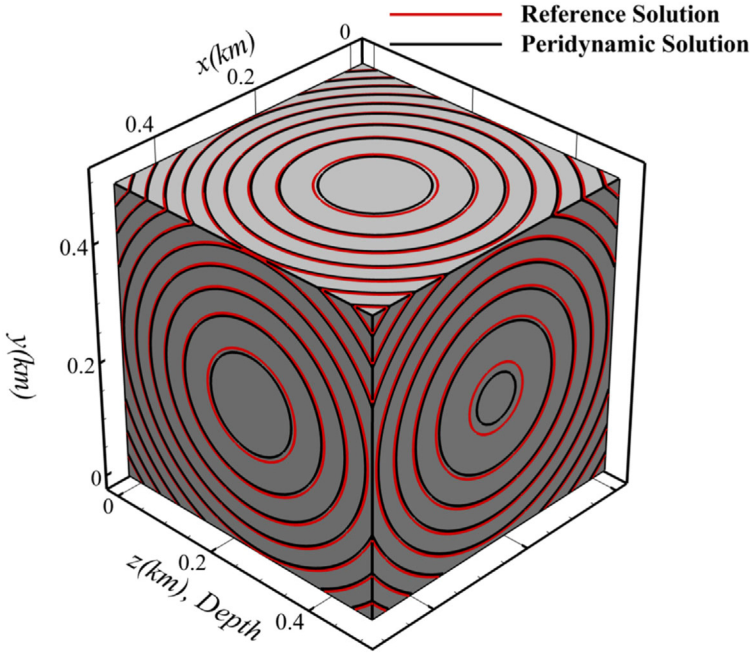

Fig. 23. Comparison of PD traveltimes predictions with the analytical solution.

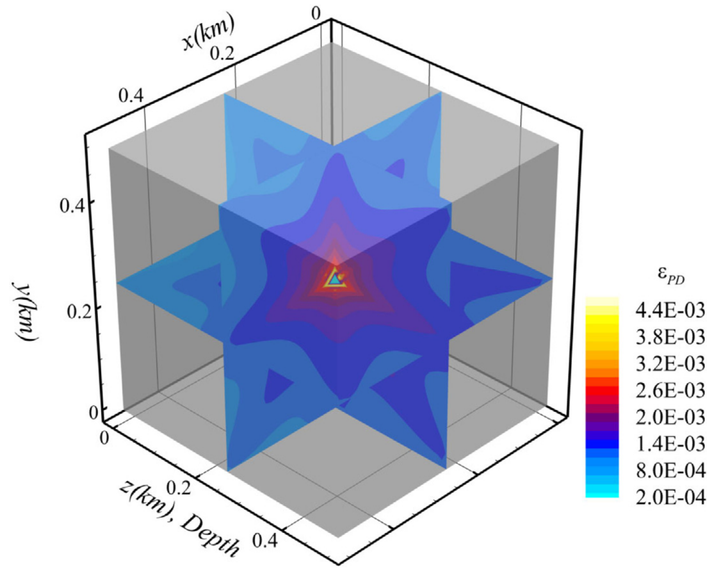

Fig. 24. Absolute error in PD solution against the analytical solution for isotropic Eikonal equation.

a unified manner without any special treatment. The results agree well with the analytical and analytical/reference solutions.

Declaration of competing interest

The authors declare that they have no known competing financial interests or personal relationships that could have appeared to influence the work reported in this paper.

Acknowledgment

This study was performed as part of the ongoing research at the MURI Center for Material Failure Prediction through Peridynamics at the University of Arizona (AFOSR Grant No. FA9550-14-1-0073), USA.

References

[1] R. Courant, E. Isaacson, M. Rees, On the solution of nonlinear hyperbolic differential equations by finite differences, Comm. Pure Appl. Math. 5 (1952) 243–255.
[2] I. Christie, Upwind compact finite difference schemes, J. Comput. Phys. 59 (1985) 353–368.
[3] R.C. Swanson, E. Turkel, On central-difference and upwind schemes, J. Comput. Phys. 101 (1992) 292–306.
[4] M. Stynes, H.G. Roos, The.midpoint.upwind. scheme, Appl. numer. math., 23 (1997) 361–374.
[5] V.G. Ferreira, R.A.B. De Queiroz, G.A.B. Lima, R.G. Cuenca, C.M. Oishi, J.L.F. Azevedo, S. McKee, A bounded upwinding scheme for computing convection-dominated transport problems, Comput. & Fluids 57 (2012) 208–224.
[6] G.A. Sod, A survey of several finite difference methods for systems of nonlinear hyperbolic conservation laws, J. Comput. Phys. 27 (1978) 1–31.
[7] R.J. LeVeque, Finite Volume Methods for Hyperbolic Problems, Cambridge University Press, 2002.
[8] N. Moës, J. Dolbow, T. Belytschko, A finite element method for crack growth without remeshing, Internat. J. Numer. Methods Engrg. 46 (1999) 131–150.
[9] H. Tian, L. Ju, Q. Du, Nonlocal convection–diffusion problems and finite element approximations, Comput. Methods Appl. Mech. Engrg. 289 (2015) 60–78.
[10] Y. Leng, X. Tian, L. Demkowicz, H. Gomez, J.T. Foster, A Petrov–Galerkin method for nonlocal convection-dominated diffusion problems, arXiv:2107.07080.
[11] H. Lee, Q. Du, Nonlocal gradient operators with a nonspherical interaction neighborhood and their applications, ESAIM: Math. Model. Numer. Anal. 54 (2019) 105–128.
[12] H. Lee, Q. Du, Asymptotically Compatible SPH-Like Particle Discretizations of One Dimensional Linear Advection Models, Vol. 57, 2019, pp. 127–147. http://dx.doi.org/10.1137/18m1175215.
[13] Q. Du, Z. Huang, P.G. Lefloch, Nonlocal conservation laws, in: A New Class of Monotonicity-Preserving Models, Vol. 55, 2017, pp. 2465–2489, http://dx.doi.org/10.1137/16M1105372.
[14] Q. Du, J.R. Kamm, R.B. Lehoucq, M.L. Parks, A New Approach for a Nonlocal, Nonlinear Conservation Law, Vol. 72, 2012, pp. 464–487. http://dx.doi.org/10.1137/110833233.
[15] Q. Du, Z. Huang, R.B. Lehoucq, Nonlocal convection–diffusion volume-constrained problems and jump processes, Discrete Contin. Dyn. Syst - B 19 (2014) 373–389.
[16] E. Madenci, A. Barut, M. Futch, Peridynamic differential operator and its applications, Comput. Methods Appl. Mech. Engrg. 304 (2016) 408–451.
[17] E. Madenci, A. Barut, M. Dorduncu, M. Futch, Numerical solution of linear and nonlinear partial differential equations by using the peridynamic differential operator, Numer. Methods Partial Differential Equations 33 (2017) 1726–1753.
[18] E. Madenci, A. Barut, M. Dorduncu, Peridynamic Differential Operators for Numerical Analysis, Springer, 2019.
[19] S. Fomel, S. Luo, H. Zhao, Fast sweeping method for the factored eikonal equation, J. Comput. Phys. 228 (2009) 6440–6455.
[20] S.A. Silling, Reformulation of elasticity theory for discontinuities and long-range forces, J. Mech. Phys. Solids 48 (2000) 175–209.
[21] J.L. Bentley, Multidimensional binary search trees used for associative searching, Commun. ACM 18 (1975) 509–517.
[22] E. Madenci, A. Barut, N. Phan, N, Peridynamic unit cell homogenization for thermoelastic properties of heterogenous microstructures with defects, Compos. Struct. 188 (2017) 104–115.
[23] F. Bobaru, M. Yang, L.F. Alves, S.A. Silling, E. Askari, J. Xu, Convergence, adaptive refinement, and scaling in 1D peridynamics, Internat. J. Numer. Methods Engrg. 77 (2009) 852–877.
[24] B. Boys, T.J. Dodwell, M. Hobbs, M. Girolami, Peripy–A high performance opencl peridynamics package, Comput. Methods Appl. Mech. Engrg. 386 (2021) 114085.
[25] A.C. Bekar, E. Madenci, Peridynamics enabled learning partial differential equations, J. Comput. Phys. 434 (2021) 110193.
[26] R.J. LeVeque, Numerical Methods for Conservation Laws, 132, Birkhäuser, Basel, 1992.
[27] J. Thomas, Numerical Partial Differential Equations: Conservation Laws and Elliptic Equations, Springer, 1999.
[28] J. Li, Z. Du, A two-stage fourth order time-accurate discretization for lax–wendroff type flow solvers I hyperbolic conservation laws, SIAM J. Sci. Comput. 38 (2016) A3046–A3069.
[29] B. Van Leer, Flux-Vector Splitting for the Euler Equation, Upwind and High-Resolution Schemes, Springer, 1997, pp. 80–89.
[30] A.C. Bekar, E. Madenci, E. Haghighat, U. bin Waheed, T. Alkhalifah, Solving the eikonal equation for compressional and shear waves in anisotropic media using peridynamic differential operator, 2021, http://arxiv.org/abs/2107.01268.